Vanyukov, V. V.; Mikheev, K. G.; Nasibulin, A. G.; Svirko, Y.; Mikheev, G. M.

Enhanced saturable absorption in the laser-treated free-standing carbon nanotube films

Published in:
Optics Letters

DOI:
10.1364/OL.399852

Published: 01/10/2020

Document Version
Publisher's PDF, also known as Version of record

Published under the following license:
Other

Please cite the original version:
Vanyukov, V. V., Mikheev, K. G., Nasibulin, A. G., Svirko, Y., & Mikheev, G. M. (2020). Enhanced saturable absorption in the laser-treated free-standing carbon nanotube films. *Optics Letters*, *45*(19), 5377-5380. https://doi.org/10.1364/OL.399852

Optics Letters

Enhanced saturable absorption in the laser-treated free-standing carbon nanotube films

V. V. Vanyukov,[1,*] K. G. Mikheev,[2] A. G. Nasibulin,[3,4] Y. Svirko,[1] and G. M. Mikheev[2]

[1]Institute of Photonics, University of Eastern Finland, Joensuu 80101, Finland
[2]Institute of Mechanics, Udmurt Federal Research Center of the UB RAS, Izhevsk 426067, Russia
[3]Skolkovo Institute of Science and Technology, Nobel 3, Moscow 121205, Russia
[4]Aalto University, Department of Chemistry and Materials Science, Aalto 00076, Finland
*Corresponding author: viatcheslav.vanyukov@uef.fi

Received 8 June 2020; revised 19 August 2020; accepted 20 August 2020; posted 20 August 2020 (Doc. ID 399852); published 21 September 2020

We demonstrate an increase of optical transmittance and saturable absorption of laser-treated free-standing single-walled carbon nanotube (SWNT) films. The combined acid and low-power non-destructive laser treatment ensures an enhancement of linear transmittance across the visible range and double-digit increase of the saturable absorption of femtosecond laser radiation at 795 nm. The saturable absorption coefficient and the ratio of saturable to non-saturable losses increase by 26% and 35%, correspondingly, while the saturation intensity decreases by 20% because of the treatment. Our analysis indicates that with the performed treatment one can significantly improve the nonlinear optical properties of free-standing SWNT-based ultrafast saturable absorbers.

https://doi.org/10.1364/OL.399852

An impressive performance of saturable absorbers (SA) based on single-walled carbon nanotubes (SWNTs) has been numerously demonstrated in solid-state [1,2], fiber [3–6], semiconductor [7,8], and waveguide [9,10] lasers operating in the telecom and near-IR range. The low saturation intensity, the sub-picosecond relaxation time of the nonlinear absorption, and the low cost of the nanomaterial make the SWNT SAs competitive with the semiconductor SA mirrors (SESAM) [11–13]. However, practical application of SWNT SAs remains questionable because the limited mechanical robustness of the SWNT films [3,4,14] usually requires incorporating them into a polymer matrix, which in turn may influence the SA performance [15,16]. Achieving mode-locking without the polymer matrix, the free-standing SWNT films will enable to suppress the non-saturable and enhance the saturable absorption at a lower saturation intensity [16,17].

The floating catalyst (aerosol) chemical vapor deposition (CVD) synthesis [18] is one of the most promising methods for obtaining pure free-standing films (FSFs) of SWNTs with defined thicknesses. In contrast to SWNTs synthesized by arc discharge [19,20] or by laser ablation [21,22], which require laborious processes of purification and dispersion in liquids before they can be transferred [23], the aerosol synthesized nanotubes can be transferred to almost any material by an easy dry transfer technique [24,25].

The advantageous electro-optical properties of SWNT FSFs fabricated by the aerosol synthesis method have been numerously demonstrated in transparent capacitive touch sensors, thin-film transistors, electrochemical sensors, bright organic light-emitting diodes, incident light polarization analyzers [24–26], and in mode-locking fiber lasers at wavelengths of 1.05, 1.32, 1.56, and 1.99 μm [15,25,27,28]. Moreover, it has been recently found (but not demonstrated) that the non-saturable absorption of SWNT FSFs may be suppressed if one removes the iron catalyst particles, which are conventionally used for the SWNT synthesis, by the low-power laser treatment in acid solution [29]. Such treatment results in the transformation of this catalyst residue into iron oxide compounds having much lower absorption cross sections [30].

In this work, we demonstrate that combining the acid and laser treatment can significantly improve the nonlinear optical properties of SWNT FSFs. Using femtosecond z-scan measurements, we reveal that with adjustment of the treatment parameters we achieve 7% suppression of the non-saturable absorption together with 26% increase of the saturable absorption of the film. To the best of our knowledge, the proposed treatment allows us to create the free-standing SWNT SAs with the best performance at the wavelength of 795 nm.

In the experiments, the aerosol synthesized SWNTs were collected at room temperature downstream of the reactor on membrane filters. By adjusting the collection time, we fabricated SWNT FSFs having a thickness of about 77 nm. The film was adjusted to have a thickness (~80 nm) [27] and transmittance (~80% at 1.5 μm) [15] similar to those of SWNTs FSFs-based SAs used in fiber lasers at 1.05, 1.56, and 1.99 μm. Moreover, we have recently demonstrated that at the required thickness the films have the optimal—in terms of the transmittance/sheet resistance ratio—optoelectronic performance [30]. The films were transferred onto a glass substrate with a 3 mm opening in the central part [see inset to Fig. 1(a)] to create FSFs. One of the films was kept pristine, while the others were exposed to acid and laser treatment in the argon atmosphere.

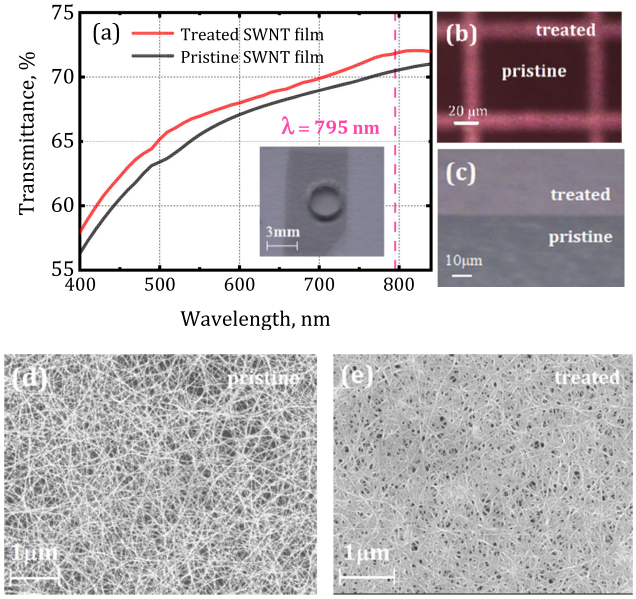

Fig. 1. (a) Optical transmittance spectra of pristine and treated (by acid and low-power laser) films. Inset shows a photo of a SWNT film transferred on the glass substrate with a hole. The substrate-free central part of the sample represents a FSF of SWNTs. (b), (c) Optical microscopy images of lines (the contrast was increased) and areas (without contrast increase) treated and pristine. SEM micrographs of (d) pristine and (e) laser-treated FSFs of SWNTs.

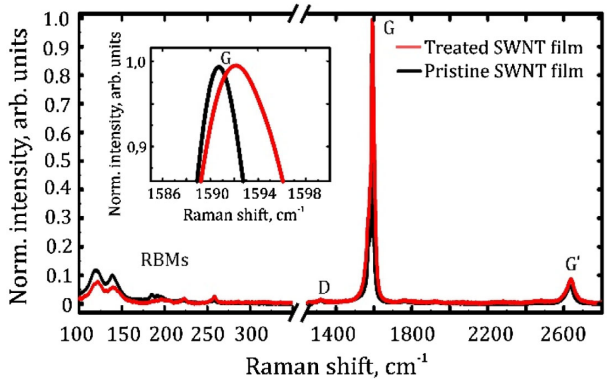

Fig. 2. Normalized Raman spectra of pristine and treated (acid and low-power laser) free-standing SWNT film. The inset shows a slight shift (~1.3 cm^{-1}) in the G-peak as a result of the treatment.

For the acid treatment, we covered the film with a thin layer of an aqueous solution of hydrochloric acid (HCl) (35 wt. %). The laser treatment was carried out by scanning the film surface by the He–Ne laser beam at 632.8 nm. Laser treatment was carried out through the 10× objective at an intensity of 3 kW/cm^2. The diameter of the laser spot (measured by a laser profiler scanning along the axis of a focused laser beam) was about 21 μm (at a level of $1/e^2$). The transmittance spectra, optical and SEM images of pristine and treated SWNT films are shown in Fig. 1.

One can observe from Fig. 1(a) that treatment resulted in the 2% increase in the film transmittance at 795 nm. The optical microscopy images shown in Figs. 1(b) and 1(c) confirm that the treated area is more transparent than non-treated. The observed transmittance increase originates from the oxidation of iron nanoparticles encapsulated in SWNT into ferric chloride ($FeCl_3$) having lower absorption losses [31]. The laser-induced decomposition arises from the reactions between encapsulated iron nanoparticles with a thin layer of HCl that we used for the treatment. The observed effect is similar to what we observed in Refs. [29,30], where acids were released from the polymer substrate due to the heat transfer from SWNTs, but without using the polymer host.

At the same time, the comparison of scanning electron microscope (SEM) images in Figs. 1(d) and 1(e) show that the treatment results in denser SWNT bundles (similar to [30]). In order to further evaluate the effect of the treatment on the SWNT structure, we compared the Raman spectra of treated and pristine films obtained at an excitation wavelength of 632.8 nm, but with much lower power density (<0.1 kW/cm^2) to avoid any possible changes introduced by Raman measurements. Both spectra presented in Fig. 2 exhibit an almost identical shape and are characterized by a typical SWNT profile, which is represented by the G-, D-, G'-peaks and the "radial breathing" modes (RBMs). A small (~1.3 cm^{-1}) shift of the G-peak from 1590.7 to 1592 cm^{-1} is observed (see inset in Fig. 2), which could be a sign of slight p-doping of SWNTs [32]. The G/D ratio of peak intensities remains unchanged (G/D = 120), which indicates that no amorphous carbon is formed during the treatment. A slight variance in RBM profiles with prevalence in both the Raman shifts of around 120 and 138 cm^{-1} indicates that the performed treatment caused no damage and/or significant change to nanotubes composing the FSF.

The nonlinear optical properties of the pristine and treated films were investigated under femtosecond pulse excitation. In the experiments, we employed a Ti:sapphire laser operating at the wavelength of λ = 795 nm with the repetition rate of 1 kHz and the pulse duration of 150 fs. Measurements were performed using the open-aperture z-scan setup, described elsewhere [33]. The transmittance $T = E_{out}/E_{in}$, where E_{in} and E_{out} are the energies of the incident and transmitted laser pulses, was measured as a function of the distance z between the SWNT FSF and the focal point. The beam waist radius measured at $1/e^2$ of the maximal intensity was $w_0 = 18.5$ μm, which corresponds to the Rayleigh length $z_0 = \pi w_0^2/\lambda = 1.35$ mm.

Figure 3 presents the normalized nonlinear transmittance $T_n = T/T_0$, where T_0 is linear transmittance of the pristine and treated SWNT FSFs measured at the incident pulse energy of $E_{in} = 20$ nJ, which corresponds to the beam intensity at the focal point of 12.4 GW/cm^2. It is worth noting that no laser-induced damage to the films was observed at intensities below 27.9 GW/cm^2 ($E_{in} = 45$ nJ). Figure 3 shows that T_n is an even function of z, $T_n(z/z_0) = T_n(-z/z_0)$. This indicates that the light-induced bleaching [34] and/or heat-induced transmittance change [35] does not occur and that transmittance of SWNT FSFs increases due to absorption saturation [11]. At $z = 0$, T_n increases by 5.05% for the pristine and 7.25% for the treated film, respectively. That is, the combined laser/acid treatment results in an enormous 43.5% enhancement of the transmittance relative to the pristine film.

In the framework of the conventional two-level model of the absorption saturation [11,17], the evolution of the light intensity inside the medium is described by the following equation:

$$\frac{dI}{dz'} = -\left[\alpha_{ns} + \frac{\alpha_0}{1 + I/I_{sat}}\right] \times I, \quad (1)$$

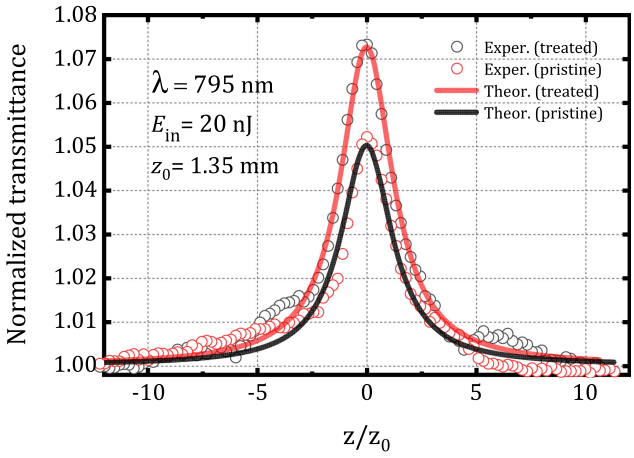

Fig. 3. Normalized transmittance of the treated and pristine FSFs of SWNTs measured in the course of z-scanning under femtosecond pulse excitation for the incident pulse energy of 20 nJ. Solid lines represent the result of the fitting with Eq. (3).

where z' is the propagation coordinate, I is the light intensity; α_{ns} and α_0 are the non-saturable and saturable absorption coefficients, respectively; I_{sat} is the saturation intensity. The solution of Eq. (1) yields [36]

$$T_n = \left[\frac{I_{out}/I_{sat} + 1 + \alpha_0/\alpha_{ns}}{I_{in}/I_{sat} + 1 + \alpha_0/\alpha_{ns}}\right]^{-\frac{\alpha_0}{\alpha_{ns}}}, \quad (2)$$

where I_{in} and I_{out} are the input and output intensities, respectively. The former depends on the SWNT FSF position z with respect to the beam waist, i.e., $I_{in} = E_{in}/(\tau \times \pi w^2(z))$, where τ is the incident pulse duration, and $w(z) = w_0(1 + (z/z_0)^2)^{1/2}$ is the beam radius. Considering that $I_{out} \approx T_0 \times I_{in}$, we arrive at the following equation describing the dependence of the normalized transmittance on the sample position:

$$T_n = \left[1 - \frac{(1 - T_0) \times \frac{E_{in}}{E_{sat}}}{\frac{E_{in}}{E_{sat}} + \left(1 + \frac{\alpha_0}{\alpha_{ns}}\right) \times \left(1 + \left(\frac{z}{z_0}\right)^2\right)}\right]^{-\frac{\alpha_0}{\alpha_{ns}}}, \quad (3)$$

where $E_{sat} = \tau \pi w_0^2 I_{sat}$.

Solid lines in Fig. 3 show the fitting of experimental data with Eq. (3) with I_{sat} and α_0/α_{ns} shown in Table 1. By using the obtained values of α_0/α_{ns} and relation $\ln T_0 = -(\alpha_{ns} + \alpha_0) \times L$, where L is the film thickness, we obtain α_0 and α_{ns}, which are also shown in Table 1. The film thickness $L = 77$ nm was calculated according to an empiric equation $L(\text{nm}) = 417 \times A_{550\,\text{nm}}$, where $A_{550\,\text{nm}}$ is the absorbance at the wavelength of 550 nm [37]. One can see from the table that proposed treatment enhances the saturable absorption coefficient α_0 by 26% (from 0.97×10^4 to 1.22×10^4 cm^{-1}), suppresses non-saturable absorption α_{ns} by 7% (from 3.58×10^4 to 3.33×10^4 cm^{-1}), and decreases the saturation intensity I_{sat} by 20% (from 7.63 to 6.34 GW/cm^2). These double-digit improvements of the nonlinear parameters confirm that the performance of the SWNT FSF-based SA can be significantly improved by the acid/laser treatment.

Table 1. Parameters Characterizing the Performance of Saturable Absorbers Based on Pristine and Treated SWNT FSFs

	I_{sat}, GW/cm^2	α_0/α_{ns}	α_0, $\times 10^4$ cm^{-1}	α_{ns}, $\times 10^4$ cm^{-1}	R
Pristine SWNT FSFs	7.63	0.269	0.97	3.58	0.23
Treated SWNT FSFs	6.34	0.366	1.22	3.33	0.31

To the best of our knowledge, there are only a few reports on mode-locking at the wavelength of 800 nm, and those are with high-pressure carbon monoxide (HiPco) SWNTs deposited on the polymer films [2,38]. At this wavelength, the saturable absorption for HiPco and aerosol synthesized SWNTs is mainly attributed to E_{22} electronic transition at ~900 nm [2,13,38], while at the telecom wavelengths it is associated with the E_{11} transition. It has been found that the saturation intensity for the E_{22} transition is higher [39] than that for E_{11}, which is around 10 MW/cm^2 (as long as the E_{11} peak matches with the wavelength) [3,17,40,41]. In our case, it is also higher compared to saturation intensity associated with the E_{11} transition. Compared to the aerosol synthesized FSFs performance at 1050 nm [27], our value is slightly lower.

Another significant parameter characterizing SAs is the saturable/non-saturable loss ratio, which can be presented in the following form [17]:

$$R = \frac{1 - \exp(-\alpha_0 L)}{1 - \exp(-\alpha_{ns} L)} \exp(-\alpha_{ns} L). \quad (4)$$

The higher the loss ratio the better the SA performance. Typically, in the SWNT-based SA, $R < 1$ [17] due to scattering on the non-resonant SWNTs [40]. The saturable/non-saturable loss ratio is a crucial parameter for application in ultrafast solid-state lasers, but not in fiber lasers, where high non-saturable losses can be tolerated due to high gain fibers [17]. The performed treatment results in an increase of the R by 35%, from 0.23 to 0.31 (see Table 1). Such a considerable increase can be explained by suppression of the non-saturable losses in the treated SWNT FSF due to removal of the catalyst residue.

Pristine aerosol synthesized SWNT FSFs have already shown their applicability as a SA for broadband mode-locking in fiber lasers [15,27,28]. The mode-locked generations were achieved using SWNT FSFs with almost the same thickness [27] and/or with similar transmittances in the IR spectral range [15] as in our study. The combined acid and low-power laser treatment makes it possible to achieve a significant improvement of the mode-locking performance of SWNT FSFs in the IR region. Moreover, the flexibility of the aerosol synthesized method provides full control of the film thickness for SA fabrication. In addition, SWNT FSFs do not contain a polymer matrix. The acid and laser treatments keep the SWNT structure intact and improve their nonlinear optical properties, paving the way towards longer-lasting SAs compatible with all-fiber laser configurations. It should be noted that a recent paper [42] reported an observation of saturable absorption enhancement by light treatment in plasmonic two-dimensional (2D) molybdenum oxide nanosheets.

In conclusion, we have demonstrated that combined acid and laser treatment of the free-standing SWNTs synthesized by the floating catalyst (aerosol) method enables the increase of the film optical transmittance by 2% across the visible range and double-digit increase of the SA characteristics at the IR region calculated by theoretical approximation of *z*-scan results using accurate equations. Specifically, at the wavelength of 795 nm, we demonstrate the increase of the saturable absorption coefficient by 26%, the decrease in the saturation intensity by 20%, and the increase in the saturable/non-saturable loss ratio by 35% compared to pristine film. Our findings open a route towards significant improvement of the mode lockers based on the free-standing aerosol SWNT films.

Funding. Academy of Finland (320165 (PREIN), 298298, 323053); Ministry of Education and Science of the Russian Federation (AAAA-A19-119021890083-0); Horizon 2020 Framework Programme (823728 (DiSetCom)); Russian Foundation for Basic Research (20-03-00804).

Acknowledgment. We thank the "Center of physical and physicochemical methods of analysis and study of the properties and surface characteristics of nanostructures, materials, and products" UdmFRC UB RAS for the use of their equipment.

Disclosures. The authors declare no conflicts of interest.

REFERENCES

1. J. H. Yim, W. B. Cho, S. Lee, Y. H. Ahn, K. Kim, H. Lim, G. Steinmeyer, V. Petrov, U. Griebner, and F. Rotermund, Appl. Phys. Lett. **93**, 161106 (2008).
2. D. Khudyakov, A. Lobach, and V. Nadtochenko, Opt. Lett. **35**, 2675 (2010).
3. S. Y. Set, H. Yaguchi, Y. Tanaka, and M. Jablonski, IEEE J. Sel. Top. Quantum Electron. **10**, 137 (2004).
4. Y. Meng, Y. Li, Y. Xu, and F. Wang, Sci. Rep. **7**, 45109 (2017).
5. X. Liu, X. Yao, and Y. Cui, Phys. Rev. Lett. **121**, 023905 (2018).
6. X. Liu, D. Popa, and N. Akhmediev, Phys. Rev. Lett. **123**, 093901 (2019).
7. Y.-W. Song, S. Yamashita, C. Goh, and S. Y. Set, Opt. Lett. **32**, 430 (2007).
8. K. Seger, N. Meiser, S. Y. Choi, B. H. Jung, D.-I. Yeom, F. Rotermund, O. Okhotnikov, F. Laurell, and V. Pasiskevicius, Opt. Express **21**, 017806 (2013).
9. G. Della Valle, R. Osellame, G. Galzerano, N. Chiodo, G. Cerullo, P. Laporta, O. Svelto, U. Morgner, A. G. Rozhin, V. Scardaci, and A. C. Ferrari, Appl. Phys. Lett. **89**, 231115 (2006).
10. S. J. Beecher, R. R. Thomson, N. D. Psaila, Z. Sun, T. Hasan, A. G. Rozhin, A. C. Ferrari, and A. K. Kar, Appl. Phys. Lett. **97**, 111114 (2010).
11. T. Hasan, Z. Sun, F. Wang, F. Bonaccorso, P. H. Tan, A. G. Rozhin, and A. C. Ferrari, Adv. Mater. **21**, 3874 (2009).
12. F. Wang, A. G. Rozhin, V. Scardaci, Z. Sun, F. Hennrich, I. H. White, W. I. Milne, and A. C. Ferrari, Nat. Nanotechnol. **3**, 738 (2008).
13. J. Wang, Y. Chen, and W. J. Blau, J. Mater. Chem. **19**, 7425 (2009).
14. J. Coleman, U. Khan, W. Blau, and Y. Gun'ko, Carbon **44**, 1624 (2006).
15. S. Kobtsev, A. Ivanenko, Y. G. Gladush, B. Nyushkov, A. Kokhanovskiy, A. Anisimov, and A. G. Nasibulin, Opt. Express **24**, 028768 (2016).
16. G. Sobon, A. Duzynska, M. Świniarski, J. Judek, J. Sotor, and M. Zdrojek, Sci. Rep. **7**, 45491 (2017).
17. S. Yamashita, A. Martinez, and B. Xu, Opt. Fiber Technol. **20**, 702 (2014).
18. A. S. Anisimov, A. G. Nasibulin, H. Jiang, P. Launois, J. Cambedouzou, S. D. Shandakov, and E. I. Kauppinen, Carbon **48**, 380 (2010).
19. S. Iijima and T. Ichihashi, Nature **363**, 603 (1993).
20. S. Karthikeyan, P. Mahalingam, and M. Karthik, E-J. Chem. **6**, 1 (2009).
21. T. Guo, P. Nikolaev, A. Thess, D. T. Colbert, and R. E. Smalley, Chem. Phys. Lett. **243**, 49 (1995).
22. A. Thess, R. Lee, P. Nikolaev, H. Dai, P. Petit, J. Robert, C. Xu, Y. H. Lee, S. G. Kim, A. G. Rinzler, D. T. Colbert, G. E. Scuseria, D. Tománek, J. E. Fischer, and R. E. Smalley, Science **273**, 483 (1996).
23. R. Das, Z. Shahnavaz, M. E. Ali, M. M. Islam, and S. B. Abd Hamid, Nanoscale Res. Lett. **11**, 510 (2016).
24. A. Kaskela, A. G. Nasibulin, M. Y. Timmermans, B. Aitchison, A. Papadimitratos, Y. Tian, Z. Zhu, H. Jiang, D. P. Brown, A. Zakhidov, and E. I. Kauppinen, Nano Lett. **10**, 4349 (2010).
25. A. G. Nasibulin, A. Kaskela, K. Mustonen, A. S. Anisimov, V. Ruiz, S. Kivisto, S. Rackauskas, M. Y. Timmermans, M. Pudas, B. Aitchison, M. Kauppinen, P. D. Brown, G. O. Okhotnikov, and I. E. Kauppinen, ACS Nano **5**, 3214 (2011).
26. G. M. Mikheev, A. G. Nasibulin, R. G. Zonov, A. Kaskela, and E. I. Kauppinen, Nano Lett. **12**, 77 (2012).
27. S. Kivistö, T. Hakulinen, A. Kaskela, B. Aitchison, D. P. Brown, A. G. Nasibulin, E. I. Kauppinen, A. Härkönen, and O. G. Okhotnikov, Opt. Express **17**, 2358 (2009).
28. A. Khegai, M. Melkumov, S. Firstov, K. Riumkin, Y. Gladush, S. Alyshev, A. Lobanov, V. Khopin, F. Afanasiev, A. G. Nasibulin, and E. Dianov, Opt. Express **26**, 023911 (2018).
29. G. M. Mikheev, K. G. Mikheev, I. V. Anoshkin, and A. G. Nasibulin, Tech. Phys. Lett. **41**, 887 (2015).
30. V. Iakovlev, Y. Sklyueva, F. Fedorov, D. Rupasov, V. Kondrashov, A. Grebenko, K. Mikheev, F. Gilmutdinov, A. Anisimov, G. Mikheev, and A. G. Nasibulin, Diam. Relat. Mater. **88**, 144 (2018).
31. B. Marian and K. Tommi, in *Fundamental and Applied Nano-Electromagnetics* (2019), pp. 59–74.
32. A. Jorio, M. A. Pimenta, A. G. Souza Filho, R. Saito, G. Dresselhaus, and M. S. Dresselhaus, New J. Phys. **5**, 139 (2003).
33. V. Vanyukov, G. Mikheev, T. Mogileva, A. Puzyr, V. Bondar, D. Lyashenko, and A. Chuvilin, J. Nanophoton. **11**, 032506 (2017).
34. G. M. Mikheev, V. L. Kuznetsov, K. G. Mikheev, T. N. Mogileva, M. A. Shuvaeva, and S. I. Moseenkov, Tech. Phys. Lett. **39**, 337 (2013).
35. P. Karlsen, M. V. Shuba, C. Beckerleg, D. I. Yuko, P. P. Kuzhir, S. A. Maksimenko, V. Ksenevich, H. Viet, A. G. Nasibulin, R. Tenne, and E. Hendry, J. Phys. D **51**, 014003 (2018).
36. G. M. Mikheev, R. Y. Krivenkov, T. N. Mogileva, K. G. Mikheev, N. Nunn, and O. A. Shenderova, J. Phys. Chem. C **121**, 8630 (2017).
37. A. L. Gorkina, A. P. Tsapenko, E. P. Gilshteyn, T. S. Koltsova, T. V. Larionova, A. Talyzin, A. S. Anisimov, I. V. Anoshkin, E. I. Kauppinen, O. V. Tolochko, and A. G. Nasibulin, Carbon **100**, 501 (2016).
38. I. H. Baek, S. Y. Choi, H. W. Lee, W. B. Cho, and V. Petrov, Opt. Express **19**, 7833 (2011).
39. J. C. Travers, J. Morgenweg, E. D. Obraztsova, A. I. Chernov, E. J. R. Kelleher, and S. V. Popov, Laser Phys. Lett. **8**, 144 (2011).
40. W. B. Cho, J. H. Yim, S. Y. Choi, S. Lee, A. Schmidt, G. Steinmeyer, U. Griebner, V. Petrov, D. I. Yeom, K. Kim, and F. Rotermund, Adv. Funct. Mater. **20**, 1937 (2010).
41. X. Liu, D. Han, Z. Sun, C. Zeng, H. Lu, D. Mao, Y. Cui, and F. Wang, Sci. Rep. **3**, 2718 (2013).
42. W. Wang, W. Yue, Z. Liu, T. Shi, J. Du, Y. Leng, R. Wei, Y. Ye, C. Liu, X. Liu, and J. Qiu, Adv. Opt. Mater. **6**, 1700948 (2018).